アノードレイヤ型ホールスラスタ UT-58 のプルーム特性および効率研究

Plume Characteristics and Efficiency Investigation of Hall Thruster UT-58 with Anode Layer

○朴俊輝(東大・院)，水川将暢(東大・学)，平野雄也，濱田悠嗣(東大・院)
小紫公也，小泉宏之，Tony Schönherr（東大）

○Junhwi Bak, Mizukawa Masanobu, Yuya Hirano, Yushi Hamada,
Kimiya Komurasaki, Hiroyuki Koizumi, and Tony Schönherr (University of Tokyo)

Abstract （概要）

To enhance anode efficiency and to reduce erosion of the UT-58 Hall thruster with anode layer, plume and efficiency characteristics' dependence on magnetic topology were investigated. To find a way to increase performance, first, the inner and outer coil ratio's effect on thruster performance was investigated. The result showed that with a larger outer coil current, inner : outer = 2 A : 5 A, plume divergence had decreased and showed the best performance; this ratio was once again confirmed with an outer coil current strength dependency test. In addition, the effect of the trim coil was tested, but it did not bring any considerable positive effect when both positive and negative current was supplied. Lastly, from the various utilization efficiencies of the UT-58: acceleration efficiency, propellant utilization efficiency, beam energy efficiency, and beam divergence efficiency, it is shown that the beam energy and divergence efficiency are the two lowest, causing low anode efficiency of the UT-58. It became clear that the plume divergence and energy utilization of TAL-type thrusters, where the ionization region is farther downstream relative to SPT-type thrusters, should be strictly taken into account to enhance thrust and anode efficiency.

Nomenclature

I : current, subscripts b for beam, d for discharge

r : radial distance

j : current density

η : efficiency

M : ion mass

$\dot{m}$: mass flow rate, subscript 'a' for anode

e : charge of an electron, 1.6 x 10^{-19} C

E_d : ion beam average energy

γ : thrust correction factor

λ_{ce} : mean free path of CEX process

σ_{ce} : CEX collision cross section

k : Boltzmann constant, 1.38×10^{-23} m^2 kg s^{-2} K^{-1}

T_n : neutral particle temperature

P : background chamber pressure

1.   Introduction

As one type of electric propulsion thrusters, Hall-effect thrusters have been researched in different countries for many years. In Japan, the project 'RAIJIN', Robust Anode-layer Intelligent thruster for Japanese IN-space propulsion system, was established in 2012 to develop a highly efficient high-power anode-layer thruster. As the first step to investigate the characteristics of the anode layer type Hall thrusters and to build an experimental database for future high-power thruster design, a 2.0 kW level Hall thruster with anode layer, hereinafter UT-58, was designed at the University of Tokyo, UT [1, 2].

A special design characteristic is that the width of the magnetic pole pieces of UT-58 can be adjusted to apply different magnetic topologies for the thruster. For instance, by having a wider gap between pole pieces, the peak of magnetic flux can be positioned outside of the channel exit, pushing the ionization region downstream leading to less erosion of the thruster walls.
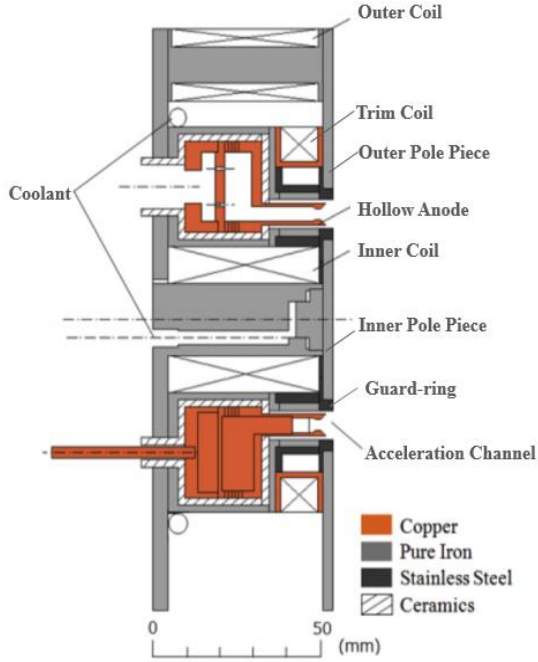
Fig. 1. Cross-section of the UT-58. Edited from Ref. 2.

As an indication of wall erosion, the ion current entering the guard-rings, refer Fig. 1, is measured. According to previous experiments[3] with two different gap widths, 14 mm and 24 mm between pole pieces, it was confirmed that the guard-ring current decreased from 14 mm to 24 mm leading to less wall erosion, however the anode efficiency was decreased as trade-off from around 60 % with gap 14 mm to around 20 % with gap 24 mm and left further investigation to find reasons for the efficiency drop. In addition, since its first development in 2013, recently UT-58 has shown the degradation of its performance with anode efficiency only up to near 20 %.

This research is to investigate the reason of the efficiency drop by figuring out multiple utilization efficiencies of the UT-58, namely, acceleration efficiency, propellant utilization efficiency, energy efficiency and plume divergence efficiency. A Faraday probe was developed for this purpose, and beam current was measured to calculate the above efficiencies. Also, the performance of the UT-58's dependence on magnetic topology coming from different combinations of inner, outer, and trim coil currents was evaluated to find the best operation point.

The Faraday probe type used is a nude Faraday probe type wherein a collector surface is directly open to an ion beam. It consists of a flat plate collector which is negatively biased to repel electrons arriving from the plasma. In addition, a guard ring is placed around the collector to prevent low energy ions coming from non-axial directions, and also to reduce

electrostatic edge effects[4]. The spacing between the collector and the guard ring is minimized to overlap the collector and the guard ring sheaths.

Beam current can be calculated by integrating the ion current density, $j(\theta)$, over the surface with the assumption of symmetry about the beam centroid.

$$I_{\mathrm{b}} = 2\pi r^2 \int_0^{\pi/2} j(\theta) \sin(\theta)\, d\theta \tag{1}$$

Here, θ is an angle between the collector and the center of the thruster, r is a hemispherical surface distance from the thruster exit.

For thruster analysis, only the anode propellant flow rate and discharge power are considered, and this can be expressed as the product of the acceleration efficiency, η_a, the propellant utilization efficiency, η_u, the energy efficiency, η_E, and the plume divergence efficiency, η_{div}.

$$\eta_{anode} = \eta_a \eta_u \eta_E \eta_{div} \tag{2}$$

$$\eta_a = \frac{I_b}{I_d} \tag{3}$$

$$\eta_u = \frac{M I_b}{\dot{m}_a e} \tag{4}$$

$$\eta_E = \frac{E_m}{e V_d} \tag{5}$$

$\eta_{div} = \gamma^2$, where

$$\gamma = \frac{2\pi r^2 \int_0^{\pi/2} j(\theta) \sin(\theta) \cos(\theta)\, d\theta}{I_b} \tag{6}$$

As mentioned in Ref. 5, because thrust weighting factor in Eq. (6), $\sin(\theta)\cos(\theta)$, peaks at 45 degrees, the composition of the beam out to at least 45 degrees is significant with regard to performance[5].

2. Experimental Apparatus and Procedure

2.1 UT-58 operation system The UT-58 operation system is shown in Fig. 2. The system was tested in the 2 m diameter, 3 m long space chamber at UT. The chamber is equipped with two rotary pumps PKS-070 (ULVAC), one mechanical booster pump PMB-060B (ULVAC), and one oil diffusion pump PFL-36 (ULVAC), yielding a total pumping speed of 37,000 liters/s. For this experiment, due to a damage on a pumping line connected to one rotary pump, only one rotary pump was used for the operation.

During the UT-58 operation, chamber vacuum pressure was measured by an ionization gauge GI-D7 (ULVAC), capable of measuring pressure in the 6.7 x 10^{-1} to 10^{-6} Pa range.
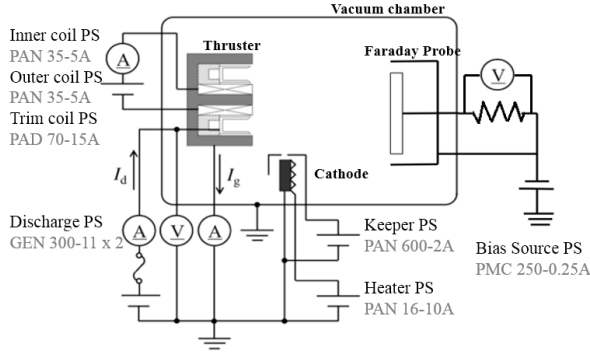
Fig. 2. Diagram of UT-58 operation system.

A hollow cathode HCN-252 (Veeco Instruments) was used as an electron source. The hollow cathode was fed with xenon, and the flow rate was set to 0.29 mg/s for all anode mass flow rate and maintained by a commercial mass flow controller model 3660 (KOFLOC).

Xenon to the thruster was fed by two a commercial mass flow controller model 3220 (KOFLOC).

The discharge characteristics data, such as discharge voltage and discharge current, and coil current data was acquired by an oscilloscope WE7000 (YOKOGAWA).

Thruster was measured by a null-displacement type dual pendulum thruster stand developed at the UT[6]. For details of the stand, refer to Ref. 6.

2.2 Faraday probe

2.2.1 Faraday probe setup The Faraday probe collector head was set at a radial distance of 210 mm from the exit of thruster and rotated from 0 deg to 85.5 deg by a step-motor. Due to the thruster setup on the stand, the range above 85.5 deg was not able to be measured, so data at 85.5 deg was used for the range from 85.5 deg to 90 deg.

All parameters to control the system, such as the arm rotation angle and the arm rotation speed are set in a LabVIEW control program, and the beam current density was measured by reading voltage on the resistance connected to the head, Fig. 2, with USB-6002 (National Instruments).

Current density data was measured 4 - 6 times, at one discharge condition, continuously by sweeping the arm from 0 deg to 85.5 deg, and from 85.5 deg to 0 deg, and their deviation was used as an error bar. In addition, current density was measured discretely once more by measuring it at certain angles, every 8.55 deg, to be used as a reference and to correct the sweeping data when it measures a higher density due to plasma disturbance.
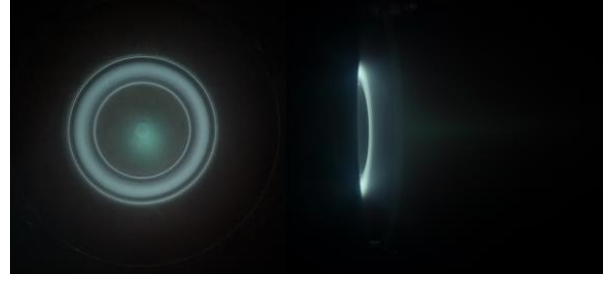
Fig. 3. UT-58 operation at inner outer ratio 2 A : 5 A and no trim coil current. It shows the plume is focused toward the center line, and the plasma is clearly detached from the guard-rings.

2.2.2 Beam current correction Due to the charge-exchange collisions between the ions and the neutral particles, the measured beam current at a certain distance from the exit of the thruster decreased. By the effect of background pressure on the beam current, the current was corrected by Eq. (7)[7].

The neutral mean free path was calculated by Eq. (8). The neutral temperature T_n was assumed 300 K, and the xenon charge-exchange cross sections σ_{ce} was calculated by Eq. (9) from Ref. 8, and for this experiment, because the ion energy E was not directly measured, it was assumed to be 90% of the discharge voltage, for instance, 180 eV for the discharge voltage of 200 V.

$$I_b(r) = I_b(0)\exp(-\frac{r}{\lambda_{ce}}) \qquad (7)$$

$$\lambda_{ce} = \frac{1}{\sigma_{ce}} \cdot \frac{kT_n}{P} \qquad (8)$$

$$\sigma_{ce} = A - B \, \log(E),$$
$$where \; A/\text{Å}^2 = 87.3, B/\text{Å}^2 = 13.6 \qquad (9)$$

2.3 Coil current ratio combination With two power supplies, PAN 35-5A, inner and outer coil currents were set separately. The trim coil current was supplied by a power supply, PAD 70-15L.

2.4 Magnetic topology simulation Magnetic topologies for each current combination are simulated by an open software Finite Element Method Magnetics (FEMM), which is a Windows finite element solver for 2D and axisymmetric magnetic, electrostatic, heat flow, and current flow problems[9].
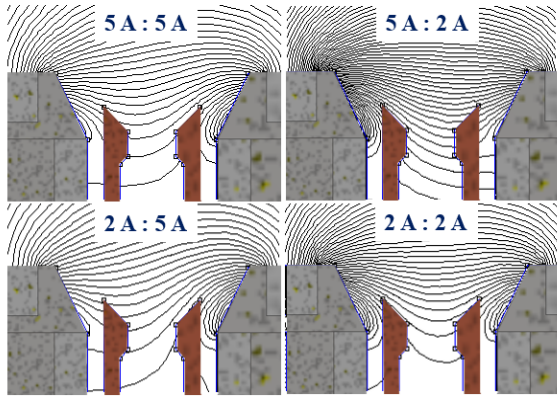
Fig. 4. Magnetic topologies by each inner/outer coil current ratio. The currents in the figure are values used in the FEMM. 2 A : 2 A shows the best topology.
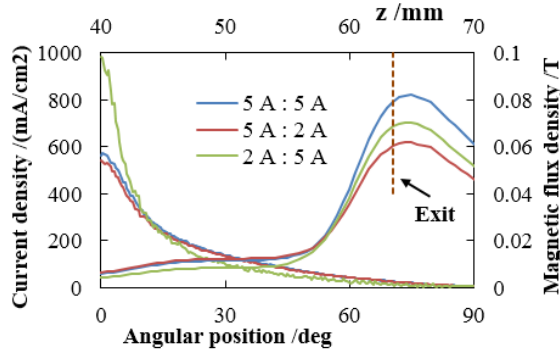
Fig. 5. Left/bottom axis : Current density by the Faraday probe. Right/top axis : Magnetic flux density along the center line. No change of the magnetic flux density peak.
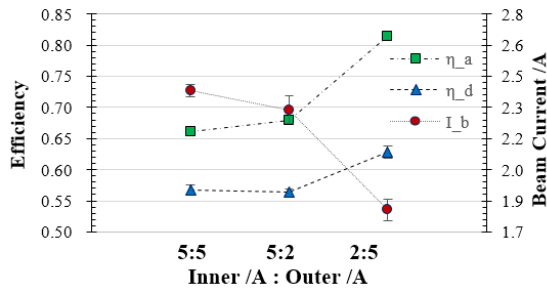
Fig. 6. Result of inner / outer coil ratio effect at $\dot{m} = 2.72$ mg/s, $V_d = 200$ V.
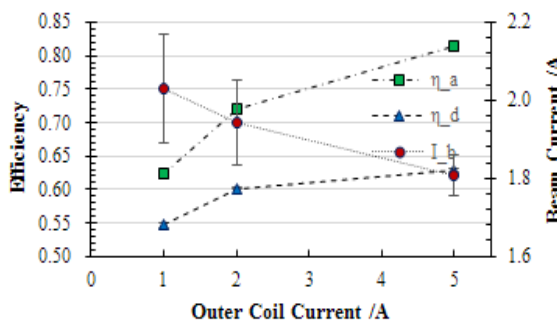
Fig. 7. Result of outer coil strength with respect to inner coil current 2 A at $\dot{m} = 2.72$ mg/s, $V_d = 200$ V.

3.   Results and Discussion

3.1   Inner / outer coil current ratio effect   The inner / outer coil current ratio effect for 5 A : 5 A,   5 A : 2 A, and 2 A : 5 A is shown in Fig. 6. With stronger outer coil current, beam current decreased from 2.4 A to 1.8 A, and so too for thrust from 27 mN to 25 mN. However, beam current ratio with respect to discharge current has increased, and eventually leads to a high acceleration efficiency increase from 0.66 to 0.82, plus the plume divergence efficiency has increased as well. The operation photo in Fig. 3 shows that the plume is focused toward the center line, and the plasma is detached from the guard-rings. From this result, it was found that for the current UT-58, stronger outer coil current than inner coil has the better performance.

However, referring the magnetic topology simulation result in Fig. 4, the result of the ratio 2 A : 2 A, bottom right in the figure, shows better symmetric magnetic topology than that of 2 A : 5 A. When UT-58 was first designed, the inner and outer coils were designed to have a 1:1 current ratio to achieve its optimized magnetic topology. However, over its operation of more than 2 years, due to deterioration of parts for the magnetic circuit, iron hematite for example, which exhibits antiferromagnetism, it seems that the optimal magnetic topology of UT-58 has moved away from a ratio of 1:1 and the better topology can be achieved with the higher outer coil current. From this result, for the simulation with the trim coil current, Fig. 8, inner and outer coil current in FEMM are set as both 2 A.

3.2   Outer coil current strength effect   As the next step, outer coil strength with respect to inner coil current fixed at 2 A was carried out and the result was plotted in Fig. 7. Similarly with the result of Fig. 6, it was observed that the efficiency increased with higher outer coil current compared to inner. Due to the limitation of the maximum 5 A that the power supply could supply to the outer coil, it was not able to supply more than that, but it was expected that the performance may increase with bigger ratio between inner and outer.

3.3   Trim coil effect   When trim coil current is a positive value, the induced magnetic field opposes the one made by the inner coil, thus expecting to trim the magnetic field by the inner coil. Magnetic topology simulation results are shown in Fig. 8. Contrary to the expectation of the effect of the trim coil which would strengthen or weaken the magnetic shielding, the induced magnetic field by the trim coil was mainly affecting
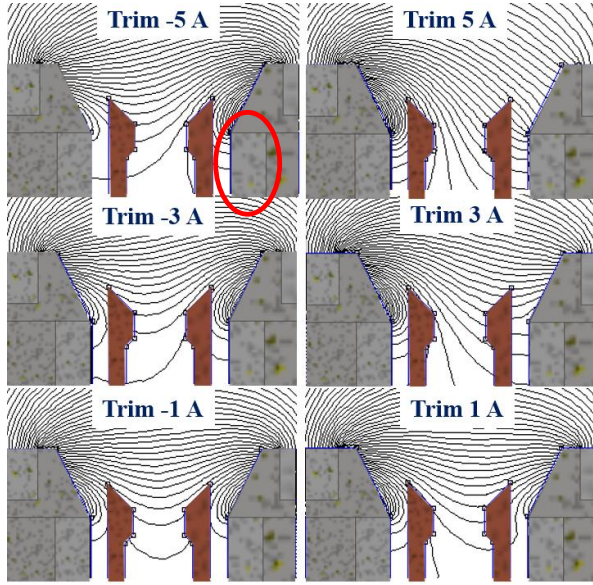
Fig. 8. Magnetic topologies by trim coil current. The currents in the figure are values used in the FEMM and the inner and outer coil current both are set as 2 A. This result shows that in most case, except -1 A, the trim coil current collapses the magnetic topology. The red circle is the outer magnetic shielding part.

the field on the outer magnetic shielding part, the red circle in Fig. 8. By strengthening and weakening the field on the region in the red, the field by the trim coil was affecting the entire magnetic topology. Only slight change was effective to achieve the symmetric well-formed magnetic topology.

Plume profiles by the trim coil current and magnetic flux density profile along the center line of the acceleration chamber are plotted in Fig. 9. From the plume angular profiles, positive trim coil current more strongly causes wide divergence, which also can be expected as well from the collapsed magnetic topologies on Fig. 8.

To reduce the interaction between plasma and the wall, the location of ionization region, which is closely related to the peak of the magnetic flux density, needs to be moved to downstream, however, it seems that the trim coil is not an effective method because the peak movement to downstream was not observed. This became clear with the experiment because the guard-ring current I_g, the indication of the wall erosion, increased when supplied the trim coil current as shown in Fig. 10.

Fig. 10 also shows how the efficiencies change relative to the trim coil current. The discharge current increases sharply as the trim coil current is supplied, leading to worse efficiencies.
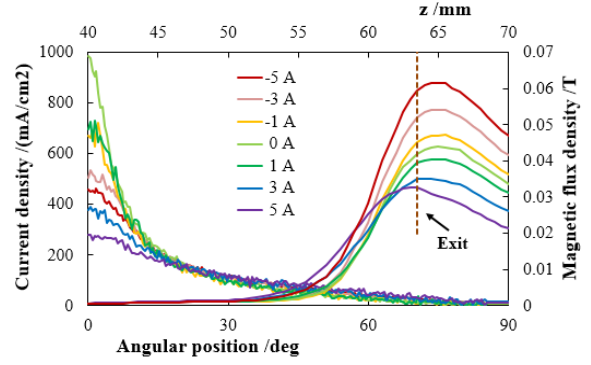
Fig. 9. Left/bottom axis : Current density by the Faraday probe. Right/top axis : Magnetic flux density along the center line by trim coil currents. The location of the peak moves upstream as the trim coil current positively increases, but not moves downstream as the trim coil current being negative.
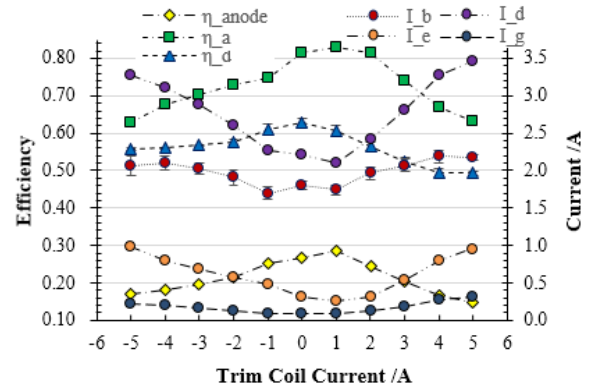
Fig. 10. Result of trim coil effect at $\dot{m}$ = 2.72 mg/s, V_d = 200 V.

Considering the increased amount of beam current and electron current, it became clear again that the trim coil is collapsing the optimal magnetic topology, and causing the magnetic field to intersect the anode and force electrons into anode as a loss as shown in the simulation result.

Even though the discharge current becomes minimum and the anode efficiency is the highest at the trim coil current 1 A, it seems it cannot overcome the negative effects.

3.4　Efficiencies and wall erosion　The utilization efficiencies and the guard-ring current versus discharge voltage is plotted in Fig. 11 at each mass flow rate. The first thing that can be noticed is that the acceleration efficiency goes over 0.8, where it is usually around 0.6 - 0.8, so it seems the backpressure effect correction may be a bit overestimated or secondary electrons emission, SEE, from the collector surface caused relatively high current. If the backpressure is
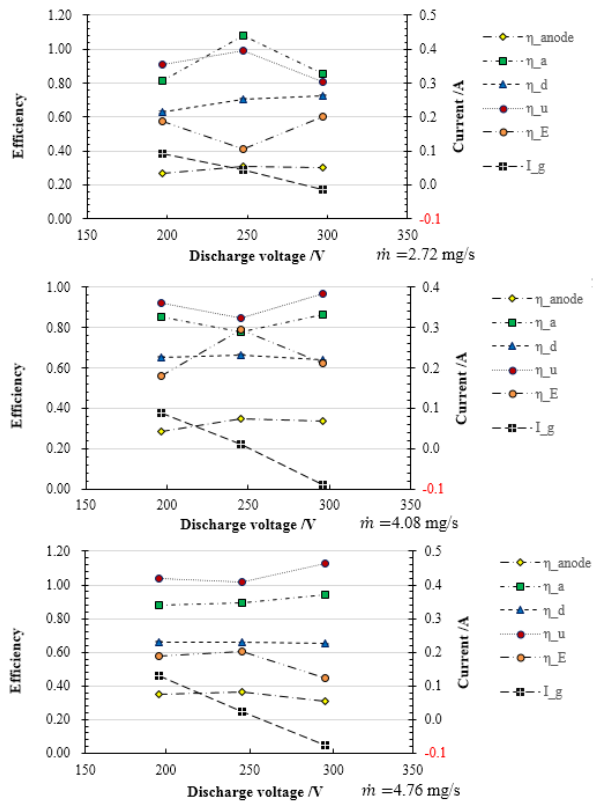
Fig. 11. Efficiencies (left axis) and the guard-ring current (right axis) vs. Discharge voltage.

From the top, $\dot{m}$ = 2.72 mg/s, 4.08 mg/s, and 4.76 mg/s.

the reason, it is necessary to measure the beam current at the different location in the chamber to see how it changes, however it has not been tested in this experiment. Rather, due to lack of a countermeasure for the electron emission on the Faraday probe, it is suspected that SEE from the collector surface mainly had influence on high current.

From Fig. 11, the acceleration efficiency is over 0.8, the divergence efficiency is 0.6 - 0.75, the propellant utilization efficiency is 0.8 - 1.1, and the beam energy efficiency is 0.4 - 0.8. What can be noticed from these results is that the beam energy utilization efficiency and the divergence efficiency are two main causes of the low anode efficiency. A probable cause is due to magnetic shielding pushing the ionization location downstream, so that beam ions cannot utilize the energy from the anode to be accelerated. In addition, it is suspected that the anode tip may be contaminated so that local charge accumulation occurred reducing the potential near the tip.

Another thing to mention is that at high mass flow rate, an inner coil current of 2 A was too low to keep stable operation, so had to be increased up to 4.5 A in case of $\dot{m}$ = 4.76 mg/s. Considering the result of inner : outer ratio, 2 A : 5 A, the ratio, 4.5 A : 5 A may not be the optimal ratio for high mass flow

rate to achieve the optimal magnetic topology. Future experiments are required to investigate how efficiencies are affected when higher current was supplied to outer coil to achieve higher inner outer ratio at the high mass flow rate.

Lastly, notice the same decreasing tendency of the guard-ring current as the discharge voltage increase. This situation implys that the ion acceleration in axial direction increases with higher discharge voltage, leading to less ion bombardment to the guard-ring. This tells the reduction of wall erosion.

4. Conclusion

The dependency of the plume characteristics, such as beam current and plume divergence, and the utilization efficiencies on magnetic topology were investigated with multiple coil current combinations and the following points were found out.

- Inner / outer coil current ratio of outer stronger shows better performance in case of the UT-58.
- Trim coil did not really have a considerable positive effect on the thruster performance by decreasing efficiencies and causing wall erosion more.
- The beam divergence efficiency and the beam energy efficiency are considered as the main reason for the low anode efficiency.
- Corresponding to discharge voltage increase, the guard-ring current decreases, leading to less wall erosion.

5. References

1) Yamamoto, N., Miyasaka, T., Komurasaki, K., Koizumi, H., Schonherr, T., Tahara, H., Takegahara, H., Aoyagi, J., Nakano, M., Funaki, I., Watanabe, H., Ohkawa, Y., Kakami, A., Takao, Y., Yokota, S., Ozaki, T., Osuga, H., Developments of Robust Anode-layer Intelligent Thruster for Japan IN-space Propulsion System. *33rd International Electric Propulsion Conference*, 2013, IEPC–2013–244.
2) Fujita, D., Kawashima, R., Ito, Y., Akagi, S., Suzuki, J., Schönherr, T., Koizumi, H., Komurasaki, K., Operating parameters and oscillation characteristics of an anode-layer Hall thruster with argon propellant, 2014, *Vacuum*, 110, 159–164.
3) Y. Hirano, J. Suzuki, T., Schonherr, R. Kawashima, S. Akagi, K. Uemoto, K. Komurasaki, H. Koizumi, The Evaluation of Magnetic Shielding in Anode-layer Type Hall Thruster, 2014, JSASS-2014-4329
4) Azziz, Y., Plasma Measurements on a 200-Watt Hall Thruster Plume, 2003, Master thesis, MIT.
5) Szabo, J. J., Robin, M., Iodine Plasma Species Measurements in a Hall Effect Thruster Plume, *49th AIAA/ASME/SAE/ASEE Joint Propulsion Conference & Exhibit*, 203, AIAA 2013–4115.
6) Nagao, N., Yokota, S., Komurasaki, K., Arakawa, Y., Development of a two-dimensional dual pendulum thrust stand for Hall thrusters, 2007, *Review of Scientific Instruments*, 78(11), 7–10.
7) Kusamoto, D., Mikami, K., Komurasaki, K., Gallimore, A. D., Exhaust beam profiles of Hall thrusters, 1998, Trans.

Jpn. Soc. Aeronaut. Space Sci, 40(130).

8) Miller, J. S., Pullins, S. H., Levandier, D. J., Chiu, Y., Dressler, R. A., Xenon charge exchange cross sections for electrostatic thruster models, 2002, *Journal of Applied Physics*, 91(3), 984.

9) D. C. Meeker, Finite Element Method Magnetics, Version 4.2 (15Nov2013 Build), http://www.femm.info